Journal of Fluids and Structures (1998) **12,** 33–45

UNSTEADY-FLOW TESTING IN A LOW-CORRECTION WIND TUNNEL

L. KONG†

Structural Department, Building Research Institute, 1 Tatehara Tsukuba City Ibaraki Prefecture, Japan 305

M. HAMEURY

Canadair Bombardier Flight Test Centre Wichita, Kansas 67209, U.S.A.

AND

G. V. PARKINSON

Department of Mechanical Engineering, The University of British Columbia, 2324 Main Mail Vancouver, B.C., Canada V6T 1Z4

(Received 15 May 1997 and in revised form 24 September 1997)

The paper describes the application of a passive low-correction wind tunnel to unsteady-flow model testing. Designed for two-dimensional (2-D) low-speed testing, the test-section has transverse airfoil-slatted side walls separating it from outer plenum chambers. The uniform spacing of the airfoil slats determines a key parameter, the open-area ratio (OAR). Two series of tests involving unsteady flow are considered, both with steady, uniform low-turbulence approach flow. In the first series, the stationary test models represent 2-D bluff bodies, three sizes of normal flat plate and four sizes of circular cylinder, the unsteady flow arising from the Kármán vortex street created in the wake of each body. Each model was tested at the same constant Reynolds number and the wake Strouhal number S was measured in a full range of tunnel wall configurations $0 \leq \text{OAR} \leq 1$, i.e. from solid walls to open jet. The results showed that, for each model, S was far too high in the presence of solid walls and too low in an open jet, while varying nearly linearly over the range of OAR. The interesting feature was that for each model shape the results for all sizes converged at a particular OAR to a value of S very close to the accepted free-air value. This success of the airfoil-slatted test-section in correcting unsteady-flow wall effects prompted the second test series to find out if oscillating test models could produce similarly successful results. The tests were on two relatively large sizes of NACA0015 airfoil in plunging oscillation, and instantaneous pressure distributions were measured for different values of oscillation amplitude and frequency over the full range of OAR. It was found that values of pressure, lift and moment coefficient close to theoretical free-air values were obtained over a small range of OAR, whereas, again, values were much too high or low, respectively, in the presence of solid walls or open jets.

†Presently at The Boundary Layer Wind Tunnel Laboratory, Faculty of Engineering Science, The University of Western Ontario, London, Ont, Canada, N6A 5B9.

0889-9746/98/010033 + 13 $25.00/fl970126

1. INTRODUCTION

A LONG-TERM PROJECT of the third author, with the help of a sequence of graduate students, has been to develop several configurations of passive low-correction wind-tunnel test-sections for different types of low-speed testing, all using a basic concept that one or more of the test-section boundaries consist of an evenly spaced row of transverse airfoil slats at zero incidence, separating the test-section from an outer plenum. The purpose of this concept, as in other passive low-correction systems, was to achieve a balance between solid boundaries (streamlines too close, model loadings too high) and open jets (streamlines too far apart, loadings too low) but without the introduction of the extra empiricism in other systems with jet flows through boundary walls containing longitudinal slots or a pattern of holes.

In the airfoil-slatted system, the only separated flow is the shear layer flowing into the plenum from the upstream solid-wall boundary layer at the entrance to the test-section. The airfoil slats operate within their unstalled range of angle of attack and potential flow modelling can be used to obtain a preliminary estimate of the best open area ratio (OAR), defined by

$$\mathrm{OAR} = \frac{g}{c+g},$$

where c is the slat chord and g the gap between slats. This system makes the flow less sensitive to the details of the test model, so that it is possible to find an OAR that will lead to low-correction data for a considerable range of sizes and shapes of models of the same class.

The first test programmes were for two-dimensional airfoils and bluff bodies, primarily using model pressure loading to measure the effects on boundary corrections of the tunnel OAR and the model size. These tests were on stationary models in uniform steady approach flow and some of the airfoil tests (Malek 1983) and all of the bluff-body tests (Hameury 1987) were carried out in the tunnel configuration used for the unsteady flow tests of the present paper.

Although the phenomena of boundary effects in unsteady flow wind-tunnel tests are very interesting, there do not appear to be very many papers, particularly about experimental research, on the subject. For example, a survey of two-dimensional wind-tunnel wall interference (Mokry *et al.* 1983) devotes only one of 10 chapters to unsteady flow effects and that deals mainly with tunnel resonance. The authors' explanation is "A more systematic presentation has not been attempted in view of an incomplete development of the theory and a lack of reliable experimental data".

It is hoped that the present paper describing two series of experiments involving unsteady flow boundary effects in the airfoil-slatted test section will be a helpful contribution, in which tunnel resonance is not a factor because of the low frequencies used in the experiments.

2. THE WIND TUNNEL

A schematic plan view of the test-section is shown in Figure 1. It is a two-dimensional insert in an existing low-speed closed-circuit tunnel. The insert is 915 mm wide by 388 mm deep in cross-section, and 2·59 m long. Test airfoil and bluff-section models are mounted vertically at the middle of the test-section. The two slatted side-wall attachments have external plenums 300 mm wide by 388 mm deep, and 2·44 m long. The airfoil slats are of NACA0015 section at zero incidence and have a 89 mm chord. They are uniformly spaced, and by

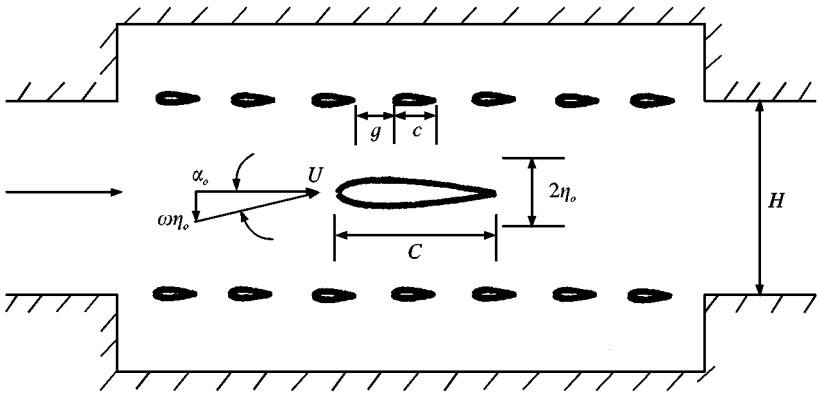

Figure 1. Plan view of test-section configuration for oscillating airfoil tests.

changing the number of slats the full range of OAR can be tested. The test-section velocity is spatially uniform within 0·3% outside the floor and ceiling boundary layers, whose displacement thickness is of the order of 8 mm at the location of the test models. The free-stream turbulence intensity is less than 0·1%.

3. KÁRMÁN VORTEX STREETS

The first series of experiments involving unsteady flow boundary effects in the tunnel configuration of Figure 1 was carried out by the second author as part of his doctoral research (Hameury 1987). The unsteady flows are organized oscillatory flows arising from the Kármán vortex streets formed in the wake of the two-dimensional bluff-body test models. The unsteady flow effects are described in the thesis, but were not included in the resulting journal publication (Parkinson & Hameury 1990), which dealt with the boundary effects on the time-averaged pressure distributions on the test models.

3.1. The Experiments

The bluff-body models tested were flat plates normal to the flow and circular cylinders. They were mounted vertically from floor to ceiling at the centre of the test-section of width H.

The sharp-edged flat plates were of three widths h: 7·6, 17·8 and 30·5 cm, corresponding to tunnel blockage ratios h/H of 8·3, 19·4 and 33·3%. A bevel was cut along the rear edges, so that the boundary layer on the front face would separate cleanly from the sharp lip. The models were equipped with pressure taps distributed over the mid-span section on the front and rear faces.

The circular cylinders were of four diameters h: 7·6, 13·7, 22·8 and 30·5 cm corresponding to h/H of 8·3, 13·8, 25·0 and 33·3%. They were made of acrylic and had very smooth surfaces with free transition. Each was equipped with pressure taps at the mid-span section. The experiments were all carried out at a Reynolds number Re of 10^5, based on the width of the flat plates or the diameter of the circular cylinders.

The model pressure taps were connected by plastic tubes to a 48-port Scanivalve. Individual pressure taps could be selected and their output fed to a Barocel pressure

transducer which transformed the input pressure into an analog electrical signal. The time-averaged surface pressure could then be read as a voltage from an averaging digital voltmeter, while the time-varying electrical signal was fed to a spectrum analyser to obtain the vortex-shedding frequencies.

Each test model was installed after calibration in the empty tunnel of a pitot tube in the nozzle, used for windspeed monitoring. Then a first wall configuration, usually the solid wall corresponding to zero OAR, was installed and the wind speed adjusted to achieve $\mathrm{Re} = 10^5$. Pressure taps were then individually selected and averaged pressures and spectral plots were obtained. Next, the process was repeated for a modified wall configuration with airfoil slats set to OAR = 0·344. When the full range of OAR had been tested, the next test model was installed and the entire procedure repeated.

3.2. Results

The results of interest here for the two model shapes are the variations with OAR and blockage ratio h/H of the Strouhal number S defined by

$$S = \frac{fh}{U},$$

where U is the approach wind speed, and f the vortex-formation frequency from one shear layer in the Kármán-wake vortex street. Figure 2 shows the results for the normal flat-plate models.

The generally acepted free-air value of S for a normal flat plate is 0·142. Figure 2 shows large departures from this in the presence of solid walls; 87% too high for 33·3% blockage, 30% too high for 19·4% blockage and still 9% too high for 8·3% blockage.

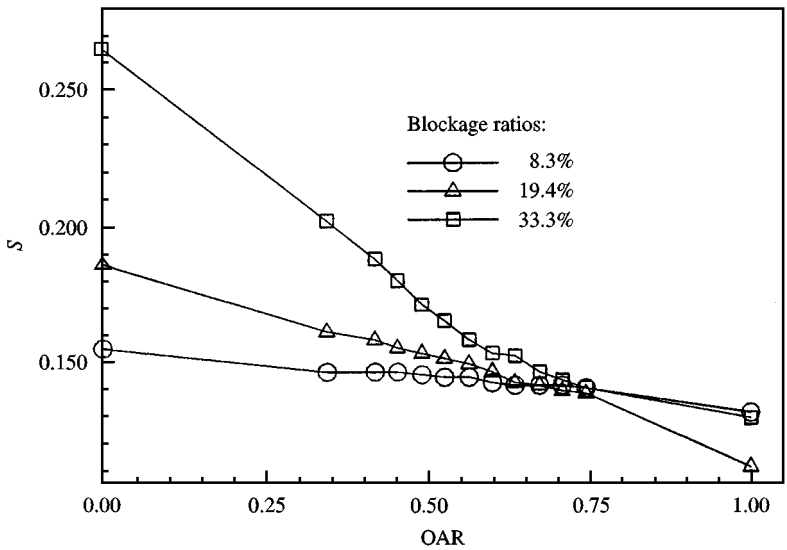

Figure 2. Variation of Strouhal number as a function of OAR for three sizes of flat-plate model positioned at the centre of the test-section.

On the other hand, in the presence of an open jet (OAR = 1) the values for all three blockage ratios are unacceptably low (although admittedly this is not an ideal open-jet configuration, since the square-end plenum boxes do not provide the usual faired collector at the downstream end of the open jet).

The tests with airfoil-slatted walls were over the range $0{\cdot}344 \leq \text{OAR} \leq 0{\cdot}745$, and the values of S for 19·4% and 8·3% blockage can be seen to converge almost linearly from the solid-wall values to the free-air value of 0·142 at OAR = 0·672. The values of S for 33·3% blockage also showed an almost linear convergence towards 0·142 over the range $0 \leq \text{OAR} \leq 0{\cdot}598$. However, at OAR = 0·635 the trend changed and the measured S at OAR = 0·672 was 0·147, 3·5% high. The probable cause is that the normal flat plate is a very bluff body, because the shear layers separate at 90° to the main flow direction and form a very broad wake. This and the 33·3% blockage were sufficient to cause flow angles into the plenum that stalled some of the airfoil slats upstream of the test model (confirmed by flow visualization using tufts on the slats) and this led to the departure from the S versus OAR trend towards convergence.

Figure 3 shows the results for the circular cylinders. Three of the cylinders were tested in the same 13 boundary configuration as the flat plates, while the smallest cylinder (8·3% blockage) was tested only for OAR = 0, 0·563, 0·635 and 0·708.

Again the results show values of S much too high in the presence of solid walls and much too low in the open-jet configuration. For the circular cylinders the flow separation is laminar at $\text{Re} = 10^5$, and occurs near 80° from the front stagnation point, so that the separating shear layers are nearly horizontal and do not create nearly as broad a wake as do the normal flat plates. As a result, the largest cylinder, with 33·3% blockage, does not stall any of the airfoil slats, and Figure 3 shows the curves of S versus OAR for the three largest cylinders converging nearly linearly to a value of $S = 0{\cdot}185$ (within the accepted range of free-air values at $\text{Re} = 10^5$) at OAR = 0·563. The four measured values of S for the smallest

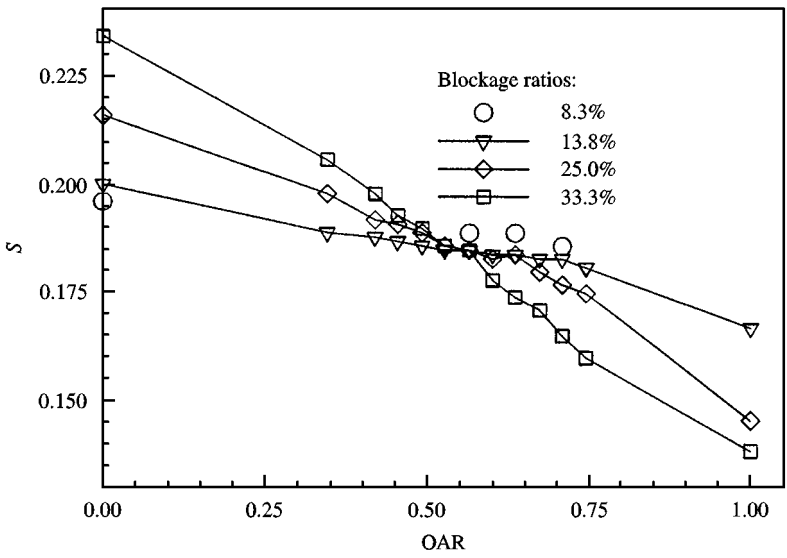

Figure 3. Variation of Strouhal number as a function of OAR for four sizes of circular cylinder model positioned at the centre of the test-section.

cylinder all appear to be somewhat high, but the value at OAR = 0·563 is 0·189, only 2% higher than the others and still within the accepted range of free-air values.

3.3 Discussion

The results indicate that the airfoil-slatted boundaries at a certain OAR, 0·672 for the flat plate, 0·563 for the circular cylinder, permit the unsteady flow created by the wake vortex street to form as it would in free air. The values of S in the presence of solid walls are too high because the wake shear layers are squeezed together so that the street vortices are closer and the frequency is higher. In the open-jet configuration the opposite is true.

The ideal OAR for the normal flat plate is higher than for the circular cylinder, because the greater bluffness of the plate produces higher outward velocities near the test-section boundaries, and they need to be more open as a consequence. Another consequence is that the results show 33·3% blockage to be permissible for testing a circular cylinder model, but too high for a normal flat plate because of the stalled airfoil slats.

The success of this form of low-correction test-section for experiments in which organized unsteady flow is created by the formation of wake vortex streets from a stationary bluff body raises the question of whether the system would also work for the flow past an oscillating test model. This led to the second series of experiments.

4. OSCILLATING AIRFOILS

This series of experiments, involving unsteady flow boundary effects in the tunnel configuration of Figure 1, was carried out by the first author as part of his graduate research (Kong 1991, 1994).

4.1. The Experiments

It was decided to test the capability of the airfoil-slatted test-section to deal with boundary corrections to the pressure loading on an oscillating body under closely two-dimensional conditions. The NACA0015 airfoil at zero incidence in low-amplitude plunging oscillation was selected as the test model. The unseparated flow would presumably produce loadings close to the predictions of potential flow, and the experimental results could be compared with the free-air values from the familiar thin-airfoil theory of Kármán & Sears (1938). Two models were used, both machined from solid aluminium, with very smooth surfaces, one of chord $C = 305$ mm and the other of $C = 610$ mm, so that the boundary interference parameters C/H were 0·333 and 0·667, respectively. Both models were instrumented with surface pressure taps in the centre plane. In the tests these taps were connected by plastic tubing to a Scanivalve and Barocel transducer, whose output was corrected, using calibration curves, for attenuation in the tubing. Airfoil displacement was measured with a linear transducer. The surface pressure at a particular tap and the airfoil displacement were measured and recorded very nearly simultaneously at successive time increments, and the process was repeated for each pressure tap using the Scanivalve, so that complete pressure distributions as a function of time over the oscillation cycle were obtained for each test condition.

The test airfoil was mounted vertically on an oscillating table under the test-section with supporting struts from the table to the bottom and around the test-section to the top of the model. The connecting struts moved through transverse slots in the test-section floor and

ceiling, which were at small clearances from the model. The oscillation mechanism for the smaller airfoil was a simple slider-crank in which, because of the small airfoil amplitudes tested, the offset was very small in comparison to the connecting-rod length, so that the airfoil oscillation was always satisfactorily close to sinusoidal. The mechanism was improved for the larger airfoil (see Section 4.3). Airfoil oscillation amplitude η_0 and circular frequency ω could be adjusted and free-stream flow velocity U controlled, so that, in the tests, reduced frequency

$$\mu = \frac{\omega C}{2U},$$

apparent angle of attack amplitude

$$\alpha_0 = \frac{\omega \eta_0}{U},$$

and Reynolds number Re were in the ranges

$$0{\cdot}25 < \mu < 0{\cdot}55, \quad 0{\cdot}2^\circ < \alpha_0 < 2{\cdot}2^\circ \quad 2{\cdot}5 \times 10^5 < \mathrm{Re} < 8{\cdot}0 \times 10^5.$$

4.2. Results

The theory of Kármán & Sears predicts that the phase angle ϕ, by which the oscillatory free-air lift, treated as a rotating vector, leads or lags the quasi-steady lift, is quite small over the range of μ covered in the present experiments (Figure 4); the experimental results indicated this to be true also for the confined flow. Therefore, the effects on phase are ignored and the effects on lift and moment amplitude only are considered. By varying μ and α_0 for the two airfoil models, seven different oscillation conditions were tested over the full

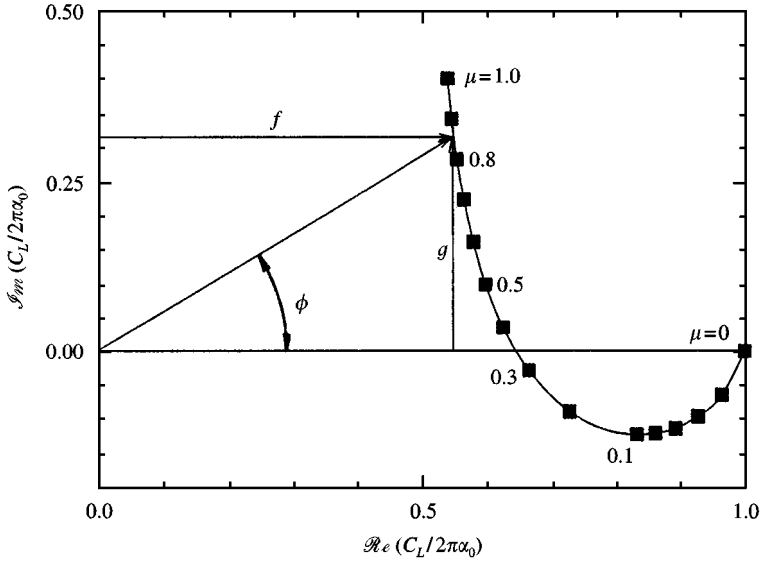

Figure 4. Loci of the real and imaginary components of unsteady lift $C_L/2\pi\alpha_0$ on a flat plate in plunging oscillation as a function of reduced frequency; $C_L = 2\pi\alpha_0$. $[f(\mu) + ig(\mu)]$.

range of OAR, as recorded in Table 1. The values of μ and α_0 in Table 1 are averages for each oscillation condition, since it was difficult to set frequency ω to the same value for each of the tests at from four to seven different OAR values.

From the oscillatory pressure traces for each tap, time-averaged amplitudes were extracted and converted to coefficients C_p. From these, the difference in loading distribution amplitudes between lower and upper surfaces, $(C_{PL} - C_{PU})$ versus X/C, was determined, and integration gave lift and moment coefficient amplitudes C_L and C_M. Figure 5 gives a sample of plots of $(C_{PL} - C_{PU})$ versus X/C for several OAR values in one of the model test conditions. The curve from the thin-airfoil theory is also shown for comparison. It can be seen that the experimental curves become progressively lower with increasing OAR, and that the curve for OAR = 0·526 lies close to the theoretical curve. Also, the experimental curve for the open-jet case (OAR = 1·0) is far more irregular than the others, indicating an

TABLE 1
Airfoil model test conditions

Symbol	C/H	$\bar{\mu}$	$\bar{\alpha}_0^0$	$\mathrm{Re} \times 10^{-5}$
●	0·333	0·52	0·62	2·5
▼	0·333	0·52	0·31	2·5
◆	0·333	0·37	0·44	2·5
▲	0·333	0·37	0·22	2·5
○	0·667	0·48	2·16	7·3
▽	0·667	0·48	1·44	8·0
△	0·667	0·28	0·82	8·0

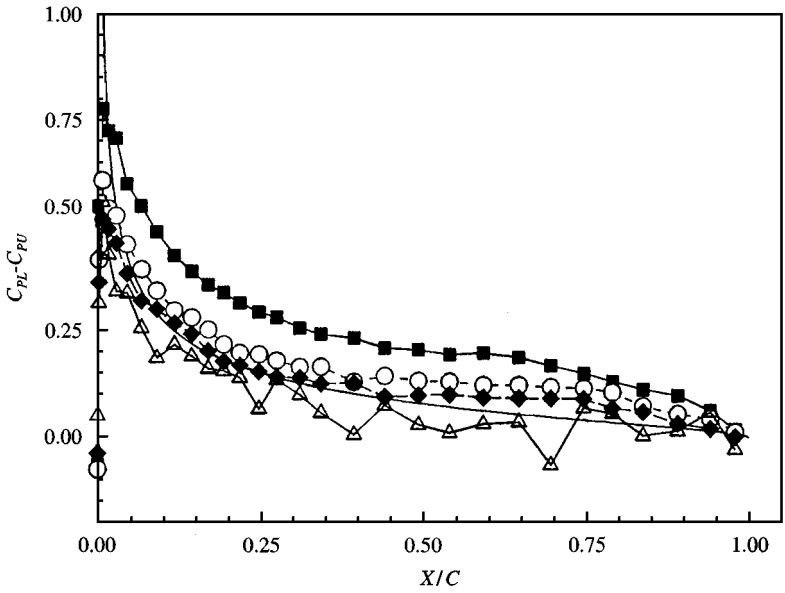

Figure 5. Pressure difference distribution along the airfoil chord for $C/H = 0{\cdot}667$, $\alpha_0 = 2{\cdot}16°$, $\mu = 0{\cdot}48$, $\mathrm{Re} = 7{\cdot}3 \times 10^5$: —, linear theory; ■, OAR = 0; ○, OAR = 0·344; ◆, OAR = 0·526; △, OAR = 1·0

appreciably lower flow quality for that test-section configuration. Integration of the curves of Figure 5 (plus three curves for other OAR values not shown in Figure 5) gives the values of lift coefficient C_L and pitching moment coefficient C_M.

The plot of C_L versus OAR in Figure 6 shows monotonic decrease in C_L with increasing OAR, as would be expected in steady-flow applications of the airfoil-slatted test-section based on earlier results (Parkinson & Hameury 1990; Malek 1983) and in agreement with the unsteady flow Strouhal number results of Figures 2 and 3. As previously indicated by the results in Figure 5, the experimental C_L for OAR $= 0{\cdot}526$ agrees closely with C_{Lf}, the theoretical free-air value in Figures 6. Figure 5 and 6 represent the same test conditions of C/H, μ, α_0 and Re. The other six combinations of parameters tested yielded similar results, and it is useful and convenient to present all the results in a collapsed form. To avoid congestion, Figures 7 and 8 present results from the four test series in which μ was near 0·5; and Figures 9 and 10 give the corresponding results from the three series in which μ was near 0·3. Moment is presented with respect to the airfoil quarter-chord, $C_{Mc/4}$, as in conventional steady-flow practice and to emphasize the apparent-mass effect on the oscillatory loading, and both C_L and $C_{Mc/4}$ are given as fractions of C_{Lf}.

In Figures 7 and 9, lift and moment are plotted versus OAR to the same scale, and in Figures 8 and 10, moment is plotted to an expanded scale to show more details. The degree to which the lift and moment data in Figures 7 and 9 collapsed to narrow bands, monotonically decreasing with increasing OAR for lift and increasing for moment, was surprising. Indeed, if all of the data had been superimposed on one figure, the lift and moment bands would not have been significantly wider, so that the method of collapse removed most of the effect of reduced frequency μ from the results. The effects of model size C/H and displacement amplitude η_0/C were qualitatively more or less as expected. At OAR $= 0$ (solid walls) the larger airfoil at its highest amplitude gave the highest value of C_L/C_{Lf} and the small airfoil at its lowest amplitude gave the lowest C_L/C_{Lf}. On the other

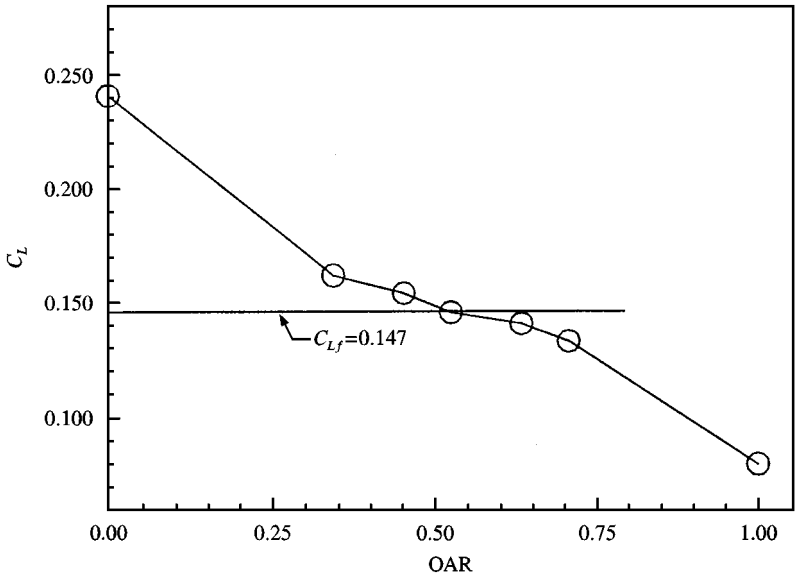

Figure 6. Lift coefficient amplitude versus OAR for $C/H = 0{\cdot}667$, $\alpha_0 = 2{\cdot}16°$, $\mu = 0{\cdot}48$, Re $= 7.3 \times 10^5$.

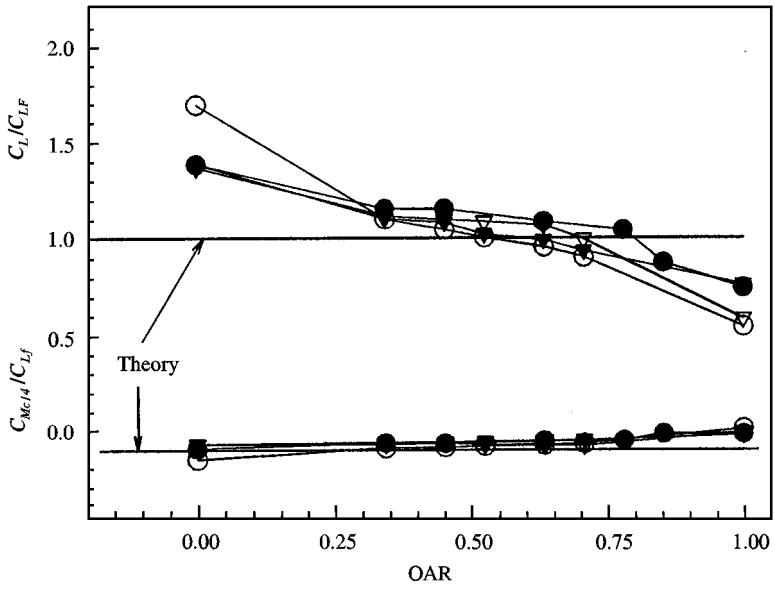

Figure 7. Collapsed lift and moment data for tests with μ near 0·5.

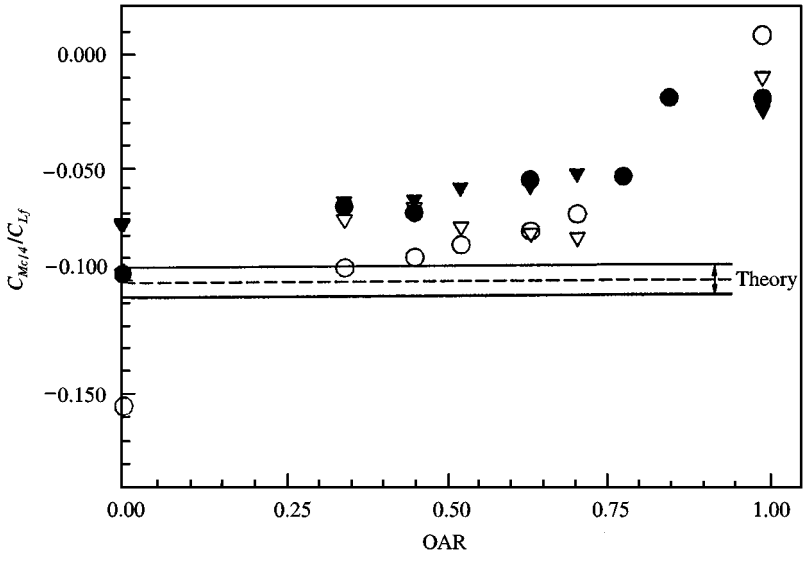

Figure 8. Collapsed moment data for tests with μ near 0·5.

hand, at OAR = 1 (open jet) the reverse was true. This is in accord with conventional boundary correction theory. However, the values of the required corrections are unexpectedly large: for lift of the larger airfoil as much as -70% for solid walls and $+45\%$ for open jet.

In the middle range of OAR, the lift data all lie close to the theoretical free-air value at $C_L/C_{Lf} = 1$. More precisely, in the range $0{\cdot}6 < \text{OAR} < 0{\cdot}8$, the average value of C_L is 2·7%

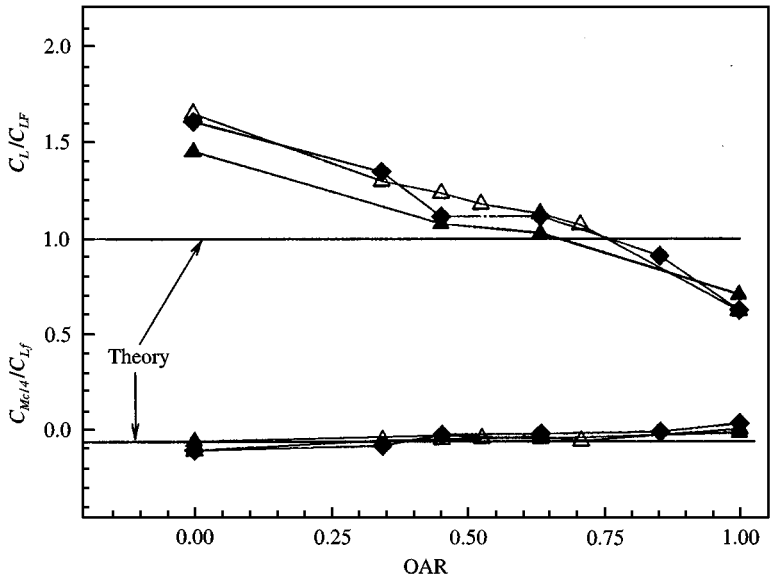

Figure 9. Collapsed lift and moment data for tests with μ near 0·3.

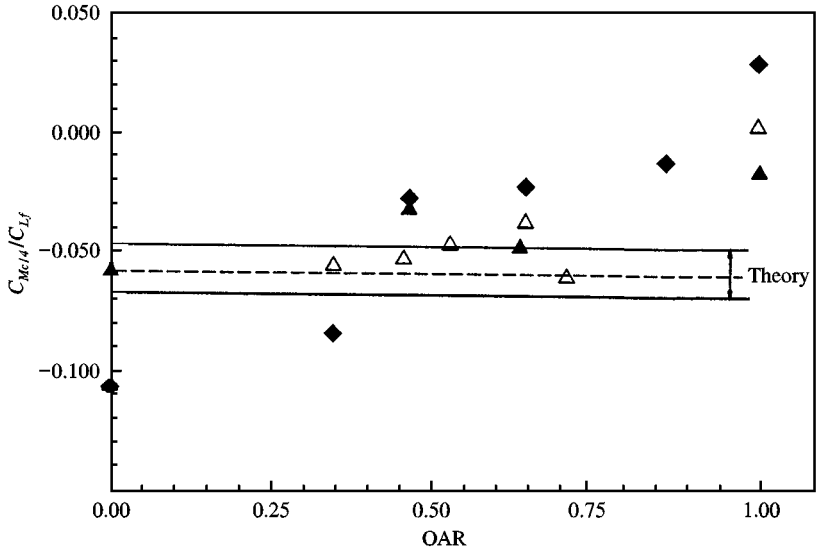

Figure 10. Collapsed moment data for tests with μ near 0·3.

higher than C_{Lf}, and at OAR = 0·708 the average value for the seven test conditions is within 1% of C_{Lf}, although individual values range from 7% high to 9% low. The moment data of Figures 7 and 9, plotted to the same scale as the lift data, fall within a very narrow band. Presented on an expanded scale in Figures 8 and 10 it can be seen, despite some scatter in both figures, to increase with OAR from negative values of the order of $-0{\cdot}1$ at OAR = 0 to near-zero values at OAR = 1. The theoretical thin-airfoil free-air values are

shown as shaded bands as a result of the dependence on μ, which varied slightly over the test range. In the mid-range of OAR the moment values are seen to be more nearly constant, and in general smaller than the theoretical values.

4.3. Discussion

The data for the smaller airfoil was obtained by the first author as part of his master's research (Kong 1991). The results were obviously interesting and encouraging, but the unexpectedly large corrections indicated for the tests in the presence of solid walls and the open jet were puzzling. The authors searched for corroborative evidence in the aerodynamics literature, but there seems to be relatively little experimental data on the plunging oscillation of airfoils. However, some was found and a report by Halfman (1952) proved useful. He suggested that serious deviations from theoretical predictions could result both from too low Reynolds numbers and too low oscillation amplitudes, and that the ratio of the boundary-layer thickness to the oscillatory displacement amplitude was an important parameter if amplitudes were small. The tests on the smaller airfoil were performed at a constant Reynolds number of $2{\cdot}5 \times 10^5$, above the lower limit of $1{\cdot}5 \times 10^5$ suggested by Halfman, but certainly the displacement amplitudes, $\eta_0/C = 0{\cdot}0052$ and $0{\cdot}0104$ were small. It was therefore decided to perform similar tests on a larger airfoil model to obtain higher Reynolds numbers, and to modify the oscillation mechanism to permit higher displacement amplitudes and exactly sinusoidal motion.

The larger airfoil, with $C/H = 0{\cdot}667$, of course posed a stiffer challenge for boundary corrections. For this second test series $\mathrm{Re} = 7{\cdot}3 \times 10^5$ and $8{\cdot}0 \times 10^5$, and displacement amplitudes η_0/C were $0{\cdot}026$ and $0{\cdot}039$. However, again to our surprise, the test results were essentially the same. The actual lift coefficients C_L were much larger, but not as a fraction of their corresponding C_{Lf}. Instead, as shown in Figures 7 and 9, the new data showed the same trends with OAR and fell in the same narrow scatter bands as the previous data. Certainly two of the three tests on the larger airfoil at $\mathrm{OAR} = 0$ and all three tests at $\mathrm{OAR} = 1$ showed larger required corrections to C_L/C_{Lf} than for the smaller airfoil, but those corrections were again unexpectedly large. One favourable effect of the new test conditions is seen in Figures 8 and 10 where, over the mid-range of OAR, the moment data-points for the larger airfoil lie closer to the theoretical band than those for the smaller airfoil. This could be a result of suppression of the boundary-layer effects mentioned by Halfman.

Further reassurance on the validity of the data seemed desirable, so the experimental method and the instrumentation were re-examined and found satisfactory.

It was therefore concluded that the data is valid, and the puzzle remains about the large values of boundary corrections for the plunging-airfoil loadings in the presence of solid walls or open jet. However, it should be noted that similar behaviour occurred in some of Halfman's data. His 2-D experiments on plunging oscillations at zero incidence used a NACA0012 airfoil in the presence of solid walls, and the measured lift and moment were compared with free-air values from thin-airfoil theory, as in the present paper. The wall-correction parameter $C/H = 0{\cdot}20$ was low enough that negligibly small corrections would be expected, and this was true at the higher of two test oscillation amplitudes, $\eta_0/C = 0{\cdot}172$, with both lift and moment data in close agreement with the free-air theory over the entire frequency range $0{\cdot}09 < \mu < 0{\cdot}31$. However, for the lower test amplitude, $\eta_0/C = 0{\cdot}086$ (still more than twice as high as the highest in the present tests, $0{\cdot}039$) the lift and moment data showed a jump in values at $\mu \simeq 0{\cdot}2$, so that over the rest of the frequency

range tested $0{\cdot}2 \lesssim \mu \lesssim 0{\cdot}4$, lift and moment values were significantly above the free-air values, lift by as much as 22% and moment by as much as 39%. The Reynolds number range for all of Halfman's tests was $7 \times 10^5 \lesssim \mathrm{Re} \lesssim 9 \times 10^5$, similar to that of the present tests of the larger airfoil with $C/H = 0{\cdot}667$.

The above facts suggest that a cause of the puzzle may be that all of the oscillation amplitudes of the present tests were too low (larger amplitudes were not possible with the apparatus used), and that boundary-layer effects play a role in the explanation, as Halfman's cautionary remarks imply.

5. CONCLUSIONS

Despite the puzzle about the unexpectedly large corrections needed for measured loadings on oscillating airfoils in the presence of solid walls and open jet, the experiments show that the airfoil-slatted boundary configuration of a 2-D wind-tunnel test-section can provide unsteady flow data requiring negligible correction for boundary effects at an optimum OAR, even for large test models. Based on these results, a suitable fixed configuration for testing 2-D bluff bodies for Strouhal number would have OAR $\simeq 0{\cdot}6$, and for testing airfoil loadings in plunging oscillation would have OAR $\simeq 0{\cdot}7$.

ACKNOWLEDGMENTS

This research was made possible by grants from the Natural Sciences and Engineering Research Council of Canada.

References

Halfman, R. L. 1952 Experimental aerodynamic derivatives of a sinusoidally oscillating airfoil in two-dimensional flow. NACA TR1108.

Hameury, M. 1987 Development of the tolerant wind tunnel for bluff body testing. Ph.D. thesis, Department of Mechanical Engineering, University of British Columbia, Vancouver, B.C., Canada.

Kármán, T. Von & Sears, W. R. 1938 Airfoil theory for non-uniform motion. *Journal of the Aeronautical Sciences* **5,** 379–390.

Kong, L. 1991 Experimental investigation of the tolerant wind tunnel for unsteady airfoil motion testing. M.A.Sc. thesis, Department of Mechanical Engineering, University of British Columbia, Vancouvr, B. C., Canada.

Kong, L. 1994 Experimental investigation of the design and testing capabilities of the tolerant wind tunnel. Ph.D. thesis, Department of Mechanical Engineering, University of British Columbia, Vancouver, B. C., Canada.

Malek, A. F. 1983 An investigation of the theoretical and experimental aerodynamic characteristics of a low-correction wind tunnel configuration for airfoil testing. Ph.D. thesis, Department of Mechanical Engineering. University of British Columbia, Vancouver, B.C., Canada.

Mokry, M., Chan, Y. Y. & Jones, D. J. 1983 Two-dimensional wind tunnel wall interference. AGARDograph No. 281.

Parkinson, G. V. & Hameury, M. 1990 Performance of the tolerant tunnel for bluff body testing. *Journal of Wind Engineering and Industrial Aerodynamics* **33,** 35–42.